JOURNAL OF PROPULSION AND POWER
Vol. 12, No. 3, May–June 1996

Global Characteristics and Structure of Hydrogen–Air Counterflow Diffusion Flames

J. Zhao* and K. M. Isaac†
University of Missouri–Rolla, Rolla, Missouri 65409-1350
and
G. L. Pellett‡
NASA Langley Research Center, Hampton, Virginia 23681

A model based on similarity transformation, for the nitrogen-diluted, H_2–air opposed-jet laminar counterflow diffusion flame (CFDF), was developed independently of earlier models, and numerically solved to study flame location and flame structure and extinction limits. Numerical stiffness is handled by a special treatment of the species production term. Flame location with respect to the stagnation plane is identified as an important parameter that governs H_2–air diffusion flames, and physical explanations are given to show how flame location is affected by fuel dilution, strain rate, and Lewis number. Results show very good agreement with experimental extinction conditions. The effect of thermal diffusion on the flame is found to be negligible. The simpler, constant Lewis number model produced extinction at half the strain rate compared to the species-dependent Lewis number model. The hydrogen–air CFDF exhibits several characteristics not observed for hydrocarbon flames. The underlying reasons are discussed in terms of the fluid dynamic and chemical kinetic aspects.

Nomenclature

A_m = constant in Eq. (14), cal-mol-K-cm-s
a = air side strain rate, $\partial u/\partial r$, 1/s
C = $(\rho\mu)/(\rho_e\mu_e)$
C_{p_i} = constant pressure specific heat i, erg/g/K
D = jet diameter, cm
D_{ij} = binary diffusion coefficient, cm^2/s
D_i^T = thermal diffusion coefficient, cm^2/s
E_m = activation energy, cal/mole
f = similarity function
h = enthalpy, erg/g
h_i^0 = formation enthalpy i, erg/g
J = number of nodes in computational domain
K = number of species; equilibrium constant
k = thermal conductivity, erg/g/s/K
k_{b_m} = backward rate constant, cal-mol-K-cm-s
k_{f_m} = forward rate constant, cal-mol-K-cm-s
Le_i = Lewis number, $\rho D_i \overline{C_p}/k$
Le_i^T = thermal Lewis number, D_i^T/D_i
n = index for flow type, $n = 0$ for two dimensional, $n = 1$ for axisymmetric, superscript for integration time level
Pr = Prandtl number, $\mu C_p/k$
p = pressure, dyne/cm^2
$\bar{R}$ = universal gas constant, erg/g/K
$\mathcal{R}_d$ = Reynolds number based on jet diameter, $\rho \bar{v}_{\text{jet}} D/\mu$
R_i = gas constant of species i, erg/g/K
R_m = gas constant of the mixture, erg/g/K
r = radial coordinate
T = temperature, K
t = time
u = velocity component in r direction, cm/s
V = diffusion velocity, cm/s
v = velocity component in z direction, cm/s
X_i = mole fraction of species i
Y_i = mass fraction of species i
z = axial coordinate
β_m = temperature exponent in Eq. (14)
η = similarity variable
θ = normalized temperature
μ = coefficient of dynamic viscosity, g/cm/s
ρ = density, g/cm^3
$\dot{\omega}_i$ = net production rate of species i, g/cm^3/s

Subscripts
e = boundary-layer edge condition; right-hand side control surface
ext = extinction condition
i = species i
j = node j in computation domain
m = serial number of the reaction in Table 1
η = derivative with respect to η

Introduction

IGNITION and extinction are of considerable importance in combustion and re-entry problems. Operational constraints often make it nearly impossible to achieve mixing at the molecular level before combustion. Thus, diffusion of fuel and oxidant into each other is a basic mechanism by which combustion takes place, and ignition and extinction are among the aspects of diffusion flame behavior most important to engine designers. Localized flame extinction characterized by the appearance of a hole in regions of high strain of the diffusion flame[1,2] has been observed in two-dimensional direct numerical simulation (DNS) of a reacting mixing layer.

Because analysis of practical systems involving diffusion flames must include realistic models for turbulence and finite rate chemistry, the structure of stretched laminar diffusion flames is being recognized as an important building block in turbulence modeling. A laminar flamelet model capable of handling finite rate chemistry has been proposed[3] for nonpremixed turbulent flames. In this approach the turbulent diffusion flame

Presented as Paper 94-0680 at the AIAA 32nd Aerospace Sciences Meeting and Exhibit, Reno, NV, Jan. 10–13, 1994; received June 12, 1994; revision received May 22, 1995; accepted for publication Nov. 20, 1995.

*Graduate Student. Student Member AIAA.
†Associate Professor, Aeropropulsion Laboratory. Senior Member AIAA.
‡Scientist, Hypersonic Applications Propulsion Branch. Member AIAA.

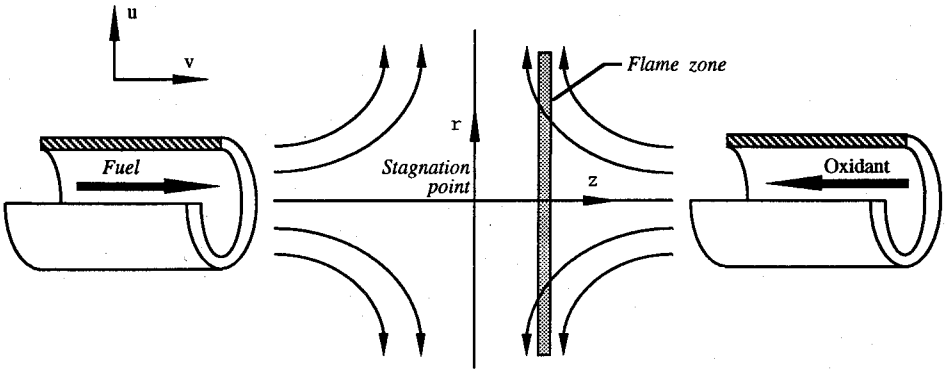

Fig. 1 Schematic diagram of the opposed-jet CFDF.

is conceived as an ensemble of thin laminar flamelets stretched and distorted by the turbulent flowfield. Application of this model requires that the length scale of the turbulent eddies must be much larger than the thickness of the reaction zone within the flamelet. Implementation of the flamelet model requires detailed knowledge of stretched laminar flames. Various laminar counter flow configurations have been extensively used in the last 30 years to study the behavior of stretched diffusion flames under conditions where the strain rate is uniform over a relatively large isothermal surface.

The objective of the present analysis is to examine how counterflow diffusion flame (CFDF) behavior is affected by input flow velocity and the composition of the fuel and airstreams. Determination of the critical values of the flowfield and chemical parameters and comparison with available experimental data is another important objective. Such validation studies can supplement evaluations of chemical kinetic data for fuel–air mixtures, especially those that are difficult to handle in the premixed flame. Finally, an evaluation of the present state of flame modeling with regard to the approximations underlying the one-dimensional model, chemical kinetics, and thermal diffusion is also an objective of present and future studies.

Laminar counterflow diffusion flames are usually formed in the laboratory by two methods: 1) by fuel and oxidant flowing towards each other from axisymmetric opposed jets[4–6] (Fig. 1) and 2) in the forward stagnation region of a cylindrical porous burner in which a fuel gas is blown into an oncoming oxidizer flow.[7] In the present analysis, the opposed-jet configuration is used to analyze the hydrogen–air counterflow diffusion flame. However, the resultant model can also be applied to the cylindrical burner with a few simple modifications of the boundary conditions.

A similarity transformation is used to reduce the governing equations to a set of ordinary differential equations (ODEs) in one independent variable; this equation set is written in the time-dependent form and solved by a finite volume, time-marching technique. A one-step second-order reaction is used to initiate the calculations, followed by the use of detailed chemical kinetic and transport property models during the second stage. Strain-induced extinction at high-velocity gradients is investigated and compared with experimental data. The effects of transport properties such as multicomponent diffusion and thermal diffusion on the flame are discussed with special reference to the use of hydrogen compared to the heavier hydrocarbon fuels.

Flame Model

Figure 1 shows the geometry considered in the present analysis. We assume the flow is laminar in the stagnation region. For the nonreacting case, an analytical solution exists for the incompressible, laminar stagnation point flow. However, as the term diffusion flame suggests, the present problem is dominated by diffusional and chemical effects; the fuel contained in one jet would diffuse into the oxidant jet and the oxidant would do likewise, establishing a narrow reaction zone in which fuel and oxidant coexist. The temperature would rise sharply at the flame. This sharp temperature peak would affect the density of the gases and the flow characteristics relative to those of the nonreacting flow. The flowfield must be determined from simultaneous solution of the equations of motion coupled with the equations of conservation of energy and species. Because the flame is restricted to a narrow region, the problem is similar to a boundary-layer-type flow in which viscous effects are restricted to the boundary layer when compared to the entire flowfield. This analogy, and the assumption that the jets are very wide compared to the zone of interest, suggests that the equations representing the counterflow diffusion flame may be transformed into a set of ODEs of the boundary-value type using a similarity transformation.

A complete description of the flowfield in Fig. 1 is given by the simultaneous partial differential equations of the conservation of momentum, energy, and individual chemical species, together with the appropriate boundary conditions. Details of the procedure used to transform these equations to the one-dimensional form are given in Refs. 8 and 9, which closely follows the formulation of Ref. 10. The final form of the equations and the boundary conditions are given next. The equation for f is of third order:

$$(Cf_{\eta\eta})_\eta + ff_{\eta\eta} + [1/(n+1)][(\rho_e/\rho) - f_\eta^2] = 0 \qquad (1)$$

The function f and its derivative f_η represent the normalized axial and radial velocities, respectively. The index $n = 0$ for planar flow and 1 for axisymmetric flow. The equations for energy and mass fractions are of second order:

$$\left(\frac{C}{Pr}h_\eta\right)_\eta + (fh)_\eta - f_\eta h + \left\{\frac{C}{Pr}\sum_{i=1}^{K} h_i\left[(Le_i - 1)Y_{i_\eta} + \frac{Le_i^T T_\eta}{T}Y_i\right]\right\}_\eta = 0 \qquad (2)$$

for $i = 1, \ldots, K-1$:

$$\left(\frac{CLe_i}{Pr}Y_{i\eta}\right)_\eta + (fY_i)_\eta - f_\eta Y_i + \left(\frac{CLe_i^T T_\eta}{PrT}Y_i\right)_\eta + \frac{1}{(n+1)}\frac{\dot{\omega}_i}{a\rho} = 0 \qquad (3)$$

The Lewis numbers used in the previous equations are defined as follows: $Le_i = (\rho D_i \overline{C_p}/k)$, and $Le_i^T = D_i^T/D_i$. For a system with K species, Eq. (3) represents $K-1$ equations. The Kth species mass fraction is obtained from the relation:

$$Y_K = 1 - \sum_{i=1}^{K-1} Y_i \qquad (4)$$

Table 1 Chemical reaction mechanism[11]

m	Chemical reactions	A_m	β_m	E_m
1	$H + O_2 \rightleftharpoons O + OH$	5.1×10^{16}	−0.82	16,150
2	$H_2 + O \rightleftharpoons H + OH$	1.8×10^{10}	1.00	8,830
3	$H_2 + OH \rightleftharpoons H + H_2O$	1.2×10^{9}	1.30	3,630
4	$OH + OH \rightleftharpoons O + H_2O$	6.0×10^{8}	1.30	0
5	$H + OH + M \rightleftharpoons H_2O + M$	7.5×10^{23}	−2.60	0
6	$H_2 + M \rightleftharpoons H + H + M$	2.2×10^{12}	0.50	92,600
7	$H + O_2 + M \rightleftharpoons HO_2 + M$	2.1×10^{18}	−1.00	0
8	$HO_2 + H \rightleftharpoons H_2 + O_2$	2.5×10^{13}	0.00	700
9	$HO_2 + H \rightleftharpoons OH + OH$	2.5×10^{14}	0.00	1,900
10	$HO_2 + O \rightleftharpoons OH + O_2$	4.8×10^{13}	0.00	1,000
11	$HO_2 + OH \rightleftharpoons H_2O + O_2$	5.0×10^{13}	0.00	1,000

Note: Units: cal-mol-K-cm-s.

From a consideration of momentum balance the following boundary condition for f can be written at $z = -\infty$ (upstream fuel side):

$$f_\eta(-\infty) = u_{-\infty}/u_\infty = \sqrt{[\rho_\infty/(\rho_{-\infty})]} \tag{5}$$

The following additional conditions are obtained from the radial velocity at the air-side edge of the solution domain and the zero axial velocity at the stagnation point:

$$f_\eta(\infty) = 1 \tag{6}$$

$$f(0) = 0 \tag{7}$$

Energy equation:

$$h(-\infty) = \sum_{i=1}^{K} Y_{i,-\infty}(h_{i,-\infty} - h^0_{i,-\infty}) \tag{8}$$

$$h(\infty) = \sum_{i=1}^{K} Y_{i,\infty}(h_{i,\infty} - h^0_{i,\infty}) \tag{9}$$

Species equations for $i = 1, \ldots, K - 1$:

$$Y_i(-\infty) = Y_{i,-\infty} \tag{10}$$

$$Y_i(\infty) = Y_{i,\infty} \tag{11}$$

Note that the coefficients appearing in the governing equations are nondimensional groups consisting of mixture density, and the transport properties of viscosity, thermal conductivity, and diffusion coefficient. Pure species viscosities, thermal conductivities, and binary diffusion coefficients were obtained from the molecular theory of gases, and the mixture viscosity and thermal conductivity were calculated using the Saxena–Wilke mixture formula. Species diffusion velocities were calculated using the multicomponent formulation,

$$V_i = \frac{1}{X_i \bar{M}} \sum_{j \neq i}^{K} M_j D_{ij} \frac{dX_j}{dx} - \frac{D_i^T}{\rho Y_i} \frac{1}{T} \frac{dT}{dx} \tag{12}$$

in which the first term on the right-hand side represents ordinary diffusion and the second term represents thermal diffusion. The derivative dX_j/dx denotes a gradient of mole fraction of species j in the x direction; and dT/dx, the temperature gradient. The symbol $\bar{M}$ stands for mean molecular weight of the gas mixture. Thermal diffusion was considered in the trace, light component limit. The transport properties were computed using the Chemkin routines[11] and the nondimensional parameters, C, Pr, Le_i, and Le_i^T appearing in Eqs. (1–3) were calculated using these transport properties. The derivatives appearing in the governing equations as coefficients were evaluated using a curve-fitting routine. The chemistry model, given in Table 1, is discussed in the Results and Discussion section.

For the numerical solution of Eqs. (1–3), the degree of variation of each of the terms in the equations was carefully examined to determine whether to choose an implicit or explicit form for it. This choice was critical for the species production term $\dot{\omega}_i$, since the stiffness associated with the present problem is reflected in this term. Because the term $\dot{\omega}_i$ is the net production rate from the forward and the backward steps in the reaction set, this term can be split into a creation term and a destruction term and handled separately to improve numerical stability.[12] Our experience showed that the finite volume technique resulted in more stable solutions compared to finite difference techniques. Calculations using a one-step model for the chemical reaction gave temperature and major species profiles, which were used as initial profiles for calculations with detailed chemistry. The solution was less sensitive to the minor species profiles. For the global time-marching procedure, initial guess profiles for temperature and species mass fractions, obtained from the one-step model, are smoothed by a commonly used curve-fitting routine. At each level in the time integration, the $L2$ norm of the mass fraction residuals is calculated as follows:

$$L2 = \sqrt{\frac{1}{(J-2)K} \sum_{j=2}^{J-1} \sum_{i=1}^{K} \left(\frac{Y_{i,j}^{n+1} - Y_{i,j}^{n}}{Y_{i,j}^{n}} \right)^2} \tag{13}$$

Note that j denotes computational node, n time level, and i species, in Eq. (13). If the $L2$ norm is greater than a specified tolerance ε, a new temperature distribution would be calculated from the enthalpy using the interval-halving method; the coefficients are then updated, and the time marching continued. The solution for one case provided initial guesses for other cases in its neighborhood; a series of solutions were obtained, each time varying the parameters only slightly. This procedure greatly reduced the computer time and effort required.

Results and Discussion

A computer program based on the previous algorithm was developed and used to investigate various aspects of hydrogen–air combustion, such as flame location, flame structure and extinction, the role of thermal diffusion of light species, and sensitivity to reaction mechanisms.

The control-volume-based algorithm is a first-order method that has large truncation errors. To establish the effect of the number of grid points, results from runs using three different grids were compared. The distribution was kept the same for all three cases to isolate the effect of the number of grid points from that of the distribution. Thus, when the number of grid points was increased from 22 to 44, a point was added at the midpoint of each interval, and for the grid with 66 points, each interval in the 22-point grid was divided into three equal segments.

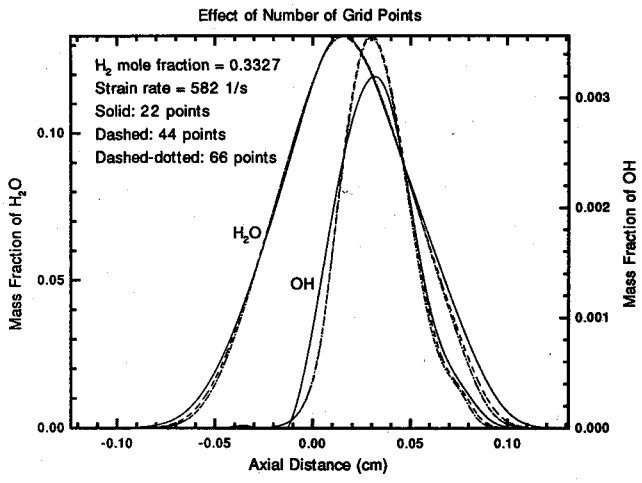

Fig. 2 Effect of grid size on the solution.

Representative results are given in Fig. 2 (also in Ref. 9), in which the Y_{H_2O} and the Y_{OH} profiles using 22, 44, and 66 grid points are compared). The comparison showed that the Y_{H_2O} profiles are almost identical for all three grids. The Y_{OH} profile for the 22-point grid differs from those for the other two, which are almost identical. Therefore, 44 points were considered sufficient for the present work to ensure grid-independent solution. Note that the temperature and velocity profiles (not given here) agreed even better than the mass fraction profiles.

The present reaction set has eight species and 22 reactions. Table 1 gives the constants for the modified Arrhenius equation for k_{f_m} (Ref. 11),

$$k_{f_m} = A_m T^{\beta_m} \exp[-(E_m/\bar{R}T)] \tag{14}$$

which represent the elementary reactions of the chemical kinetics model. The third body efficiencies are as follows: reaction 5: $H_2O = 20$; reaction 6: $H_2O = 6$, $H = 2$, $H_2 = 3$; and reaction 7: $H_2O = 21$, $H_2 = 3.3$. Third body efficiency = 1 is assumed for the remaining species. The constant k_{b_m} is calculated from the following expression in terms of the equilibrium constant K_m:

$$K_m = k_{f_m}/k_{b_m} \tag{15}$$

The equilibrium constant is calculated from the Gibbs free energy for each reaction.

Although there is no consensus yet among the various groups regarding a universal reaction mechanism to be used, the reactions shown in Table 1 have been widely used with a fair degree of success.[11] More recently, revised reaction sets have been developed for scramjet combustion[13] (NASP model). For the present, we have adopted the model given in Table 1 because it has been successfully used in the past by others.[11] Evaluation of different chemical kinetic models will be a necessary aspect of future studies.

A discussion of the flame location in relation to the fluid dynamic effects is given first. Next, the dependence of flame location on flame stretch, reactant composition, and species diffusivity is discussed, and this is followed by details of the flame structure. In the profile plots, $z = 0$ corresponds to the stagnation point (see Fig. 1). The physical rather than the transformed coordinate is used, accomplished by a reverse transformation of the coordinates from η to z, to facilitate comparison with experimental data. Flame thickness, and the maximum values of temperature and species mass fractions and their relative locations, are discussed along with mass fraction and net production rate profiles. Extinction strain rate was obtained by making runs with progressively increasing strain rate and plotting temperature vs strain rate.

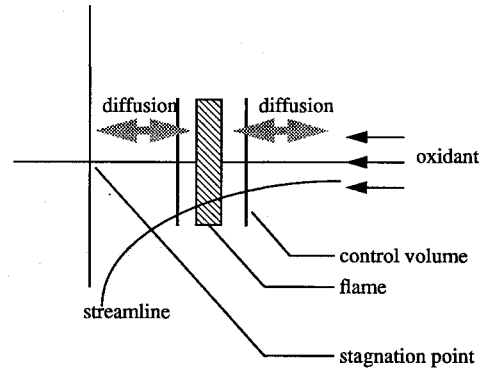

Fig. 3 Control volume showing convective–diffusive balance.

Flame Location

The counterflow diffusion flame represents an interaction of fluid dynamic and combustion processes. Because the diffusion flame lacks a well-defined characteristic such as the burning velocity of a premixed flame, a single parameter to describe diffusion flame behavior has not been identified. However, the flame location with respect to the stagnation point appears important in the description of diffusion flame behavior. The convective velocity in an H_2–air counterflow diffusion flame can vary in the range of 0–300 cm s^{-1}, depending on fuel-stream composition and input stream velocity. The flame responds to varying conditions of the fuel and oxidant streams by adjusting its position to provide the convective–diffusive balance. These facts have been obscured in the past because of the emphasis, in most experimental as well as analytical studies conducted so far, on hydrocarbon fuels for which unity Lewis number has often been assumed. Unity Lewis number is closer to reality for hydrocarbon flames than for hydrogen flames. The higher diffusion velocity of hydrogen causes the flame to locate farther towards the oxidant side, compared to a hydrocarbon flame. Qualitative descriptions of experimentally observed flame position can be found in the literature.[7,16] Fluid dynamic aspects of stretched premixed flames are given in Ref. 17. Quantitative experimental data on flame location, however, have not been reported in literature to the best of the authors' knowledge. An analytical expression for the flame location under the Burke–Schumann assumptions is given in a previous work.[18] However, a physical description of the process would be helpful to explain experimentally observed flame behavior[14] with respect to its location.

A physical description of the flame behavior is aided by considering a control volume enclosing the flame, as shown in Fig. 3. The first observation is that, in general, the flame would not always be located at the stagnation plane. Under the assumption of fast chemistry, the flame would be established where the mass fluxes of fuel and oxidant are in stoichiometric proportions. Fuel and oxidant fluxes into the control volume are from both convection and diffusion. In Fig. 3, the flame is on the oxidant side of the stagnation plane. To predict the direction of flame movement because of composition change in the reactant streams, consider a decrease in the mass fraction of fuel in the fuel stream. This will cause a decrease in the fuel mass flux by diffusion into the control volume. To satisfy stoichiometry, the rate of flow of oxidant into the control volume must also decrease. It is clear from Fig. 3 that this can be accomplished by movement of the flame towards the stagnation plane. As a result, the convective velocity at the flame would decrease because of the divergence of the streamlines; the oxidant mass flux into the control volume would also decrease proportionately. The stoichiometry surface, and hence, the flame, would now be closer to the stagnation plane. Other effects such as changes in the diffusional flux of the oxidant may be considered secondary compared to its convective flux and can be neglected in this argument.

Next, the dependence of the flame position on flow velocity (and flame stretch) may also be explained. Consider the case in which the oxidant-stream velocity increases. Convective transport of the oxidant into the control volume would increase, while fuel mass flux into the control volume would decrease because the fuel diffusion now would have to overcome the higher convection velocity to reach the flame. Again, to satisfy stoichiometry, the flame would move towards the stagnation plane where the convective velocity would be lower. The flame sheet model yields the following expression for flame location[18,19]:

$$\operatorname{erf}\left(\frac{\eta_{\text{flame}}}{\sqrt{2}}\right) = \frac{Y_{H_2,-\infty} - Y_{O_2,\infty}/r}{Y_{H_2,-\infty} + Y_{O_2,\infty}/r} \tag{16}$$

where r denotes the stoichiometric oxidant-to-fuel mass ratio ($r = 8$ for H_2-O_2 chemistry). Note that η is the transformed coordinate. Since η is a monotonically varying function of the physical coordinate z, the following argument is true in the physical plane as well. The previous expression clearly indicates that a pure H_2–air flame would be farther away from the stagnation plane than a pure hydrocarbon–air flame such as methane ($r = 4$). These findings agree qualitatively with experimental data on hydrocarbon and hydrogen flames.[4,14] The second point to note from Eq. (16) is that η_{flame} is not a function of the strain rate a. Therefore, the flame will be stationary in the η plane with respect to variations in strain rate. However, z and η are related in the transformation relation in the following manner:

$$\eta \propto \sqrt{a} \int_0^z \frac{\rho}{\rho_e}\, dz \tag{17}$$

Therefore, if the density variation is ignored for the time being, we can write:

$$z_{\text{flame}} \propto \eta_{\text{flame}}/\sqrt{a} \tag{18}$$

This agrees with the earlier physical explanation of why the flame moves closer to the stagnation plane in the physical domain as the strain rate increases. Experimental data, as well as predictions from the present one-dimensional model with detailed chemistry, show that the behavior predicted by the simpler analysis is still qualitatively correct in a real flame in which the density is not constant, Lewis numbers are not equal to unity, and the chemistry cannot be described by the Burke–Schumann model. According to the foregoing argument, a pure $CO-O_2$ flame ($r = 0.57$) should lie on the fuel side of the stagnation plane. It would be insightful to see experimental evidence of this.

Flame Structure

A diluted-fuel, low-stretch case ($X_{H_2} = 0.21$, $a = 100\ s^{-1}$, Fig. 4) is selected for discussion in this section. In the following discussion, the forward reactions in Table 1 are denoted by R1 to R11, and the reverse reactions by −R1 to −R11.

The maximum temperature (Fig. 4a) is about 1370 K and it is located slightly to the air side of the stagnation point. The H_2O, H, OH, and O maxima of the mass fraction profiles (Figs. 4b and 4c) also lie close to the temperature maximum and, therefore, any of these maxima can be used to specify flame location. An interesting feature of this case is that the profiles (except the production rates) are nearly symmetric with respect to their maxima. The probable reason for this near symmetry is that the nitrogen diluent is approximately in equal proportions in the fuel and the oxidant streams. Therefore, the thermodynamic and transport effects will tend to balance on both sides of the flame. The net species molar production rate profiles are given in Figs. 4d and 4e. The mass fraction profiles and the net production rate profiles can be used to extract information on the flame structure. To do that first consider the variations of Y_{H_2} (Fig. 4b), Y_H (Fig. 4c), $\dot{X}_{H_2}$ (Fig. 4d), and $\dot{X}_H$ (Fig. 4e). These variations can be explained in terms of the H_2-dissociation reaction (R6, Table 1). Molecular hydrogen would diffuse to the flame zone where it would encounter high temperature and dissociate into atomic hydrogen according to the forward reaction R6. Atomic hydrogen, thus formed, would diffuse to either side of the flame. On the fuel side this atomic hydrogen would recombine to form molecular hydrogen according to the reverse reaction, −R6. This is indicated by the small positive values of $\dot{X}_{H_2}$ initially on the fuel side. Also on the fuel side, the ratio of production rates, $\dot{X}_H/\dot{X}_{H_2} \simeq -2$, is the same as the ratio of the stoichiometric coefficients for reaction −R6, confirming that the three-body recombination reaction of atomic hydrogen (−R6) dictates these variations. On the oxidant side, $\dot{X}_{H_2}$ does not become positive. This may be explained in terms of the chain-branching reaction R1. This step provides the OH radicals for the formation of H_2O in steps R3, R4, and R5. The shoulder on the right of the $\dot{X}_{H_2O}$ profile in Fig. 4d may be accounted for in terms of these three reactions.

Another very interesting observation concerning this case is that the mass fraction (Fig. 4c) and the net production rate (Fig. 4e) of the chain carriers OH and O vary in near unison. Note that OH and O mass fraction profiles (Fig. 4c) have nearly the same maxima and, since their molecular weights are nearly the same, their mole fraction profiles also will have nearly the same maximum values. These nearly identical variations are consistent with the dominance of the reaction R1. Because of the high temperature in the flame, the forward step, R1 dominates, indicated by the positive values of $\dot{X}_{OH}$ and $\dot{X}_O$, whereas, to either side of the flame, the temperature drops and $\dot{X}_{OH}$ and $\dot{X}_H$ assume negative values indicating the predominance of the backward step, −R1.

Lewis Number Effects

Several numerical experiments were conducted to ascertain the effect of assuming Lewis number $(\rho D_i \overline{C_p}/k) = 1$ in simplified simulations. The most significant result is the reduction in extinction strain rate by 50% when the unity Lewis number is used, compared to a fully iterative calculation of Le_i for each species using transport properties obtained from Chemkin.[11] The solid lines in Fig. 5 are for the baseline case ($X_{H_2} = 1$, $a = 582\ s^{-1}$), and the dashed lines show the effect of assuming $Le_i = 1$ for each species. The effect is substantial. At $a = 582\ s^{-1}$, the flame is at 0.09 cm compared to 0.15 cm for the baseline case, consistent with the explanation given earlier that higher diffusion velocities and, hence, higher Lewis numbers $(\rho D_i \overline{C_p}/k)$, will shift the flame further to the oxidant side. For $Le_i = 1$, the maximum temperature is 1640 K, compared to 1900 K for the baseline case, and the flame thickness is significantly reduced (by ~0.1 cm). The radical species mass fraction profiles (Fig. 5d) and the production rate profiles (not given here) are also shifted and altered. The maximum H_2O mass fraction is reduced from 0.25 to 0.2. A similar dependence of temperature on Lewis number has been observed in a numerical simulation of hydrogen–air jet diffusion flame.[20]

A pattern can now be discerned that increasing the strain rate has the same effect, in general, as reducing the Lewis number (and mass diffusivity). Convection velocity increases with strain rate and diffusion velocity increases with Lewis number. Therefore, either increasing the strain rate or decreasing the Lewis number has the same effect of upsetting the convective–diffusive balance at the flame, which is reflected in such flame characteristics as its location, thickness, and extinction state.

One concern regarding the use of hydrogen fuel is the possible influence that thermal diffusion of light species such as H_2 and H has on flame characteristics, especially in scramjet applications. The results of a case study are compared in Ref. 9. These comparisons demonstrate that the only influence of

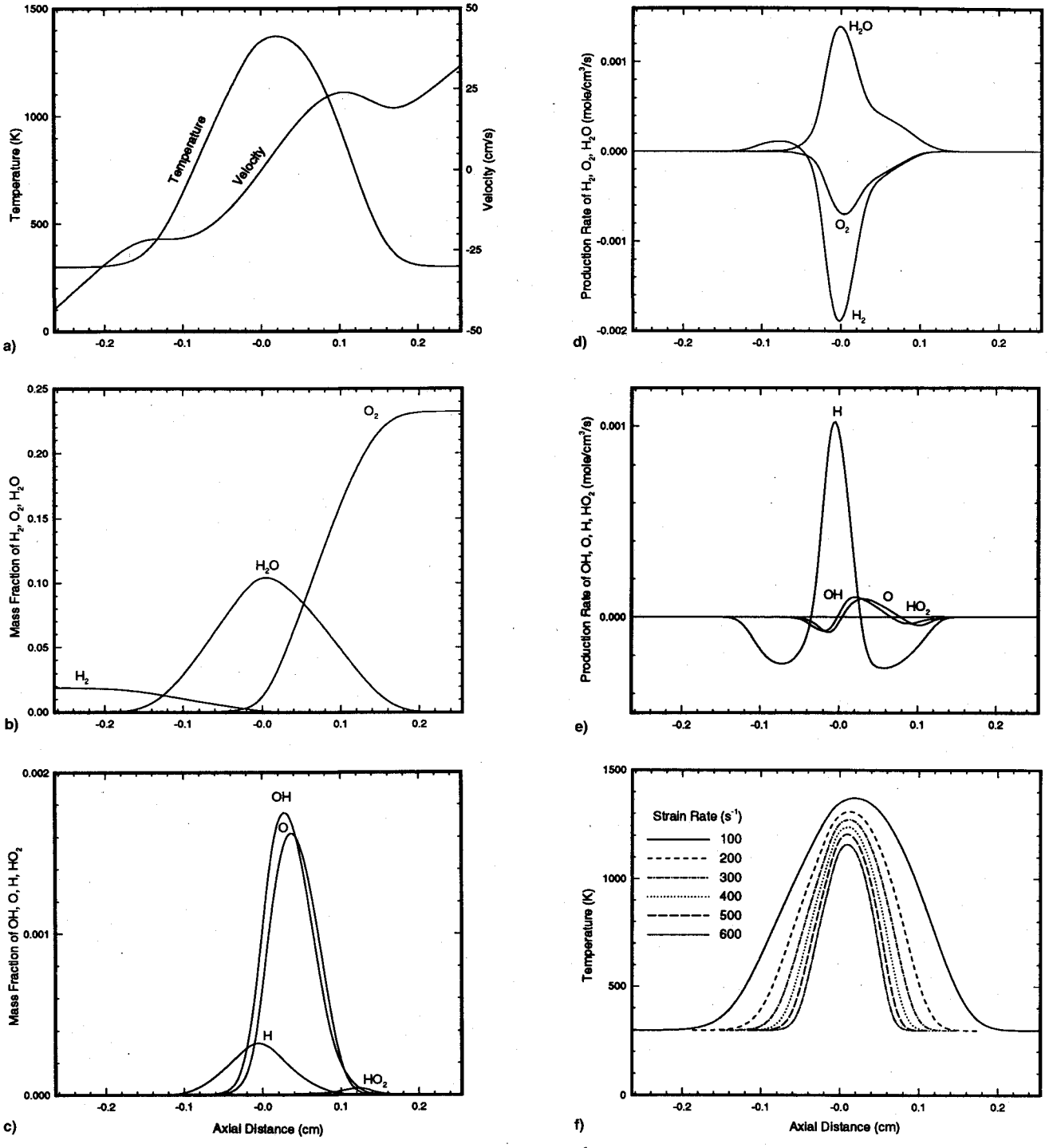

Fig. 4 a–e) fuel-lean, low-stretch case. $X_{H_2} = 0.21$, $a = 100\ s^{-1}$; and f) effect of stretch on temperature profile.

thermal diffusion on the flame is a slight reduction in peak temperature. Use of a more detailed model for thermal diffusion should not have any noticeable effect on the flame.

Comparison with Experimental Results

The measured flame structure and the present predictions have been compared in Ref. 5. Temperature and species profile comparisons in the mixture fraction space showed good agreement between experiments and predictions. The disagreement in the temperature profiles observed towards the fuel side is believed to have been caused by preheating of the fuel jet in the experiments.

Numerous opposed-jet burner (OJB) experiments have been conducted by Pellett et al.[4,15] Circular tubes and (more recently) convergent nozzles were used to obtain parabolic and plug flow profiles, respectively, at the exit. The burner was bathed in argon to prevent extraneous combustion outside the central impingement zone, which would hinder flame visibility. All measurements were made at atmospheric pressure. A digital mass flow metering system was used to measure flow rates. The flame was generally dish-shaped with its convex side facing the fuel stream. Because of the large difference between the momenta of the two streams, the flow rates of fuel and air were adjusted such that a free-floating (not anchored) flame was centered between the tubes spaced two tube diameters apart. The flow was always laminar. The fuel and airflow rates were increased slowly until extinction occurred, at which time the volume flow rates of hydrogen, nitrogen-diluent, and air were recorded. Extinction was indicated by the abrupt rupture of the flame at the axis; instead, the residual flame assumed a

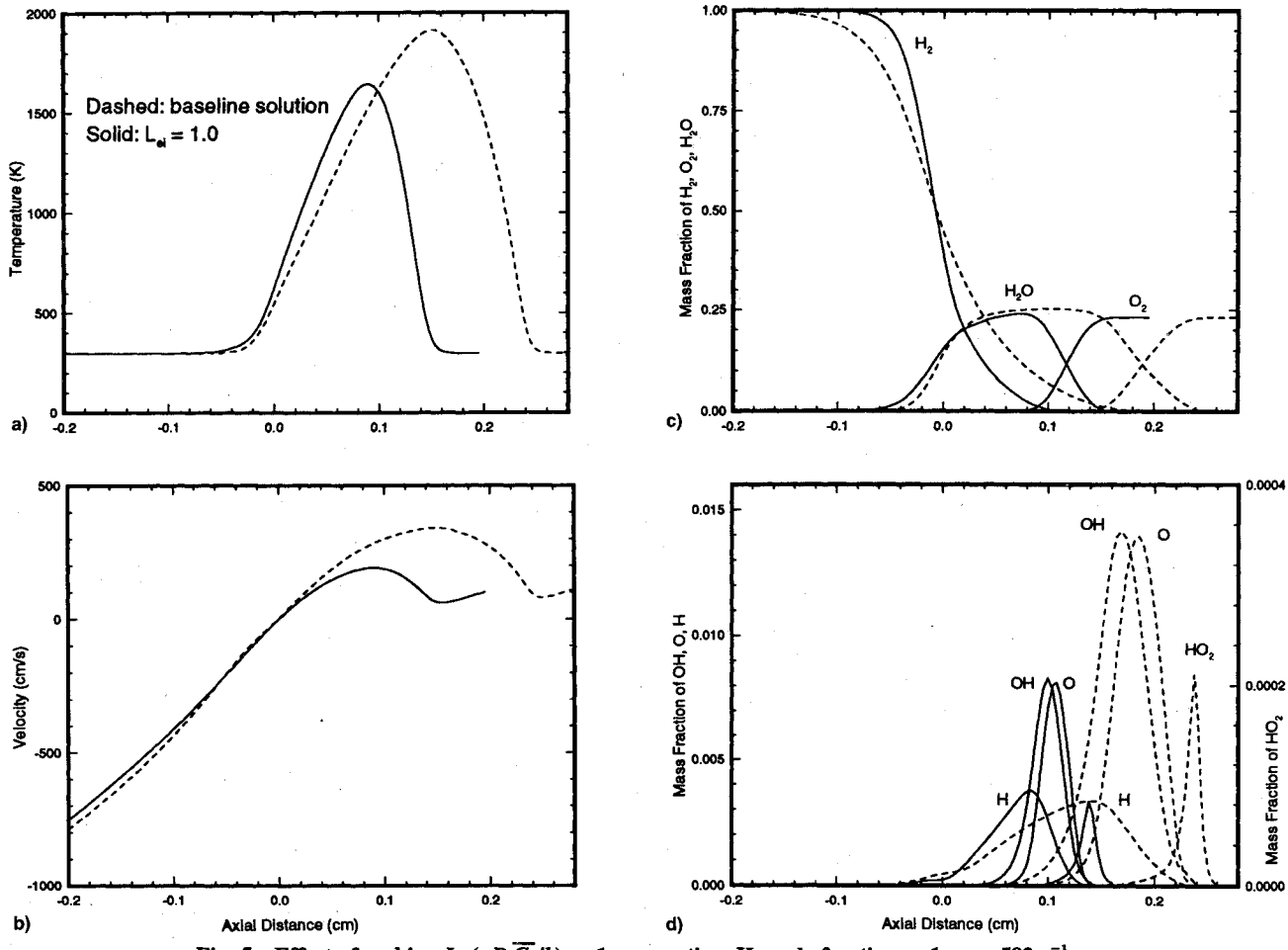

Fig. 5 Effect of making $Le_i(\rho D_i \overline{C_p}/k) = 1$ assumption. H_2-mole fraction = 1, a = 582 s^{-1}.

torus shape. The reactant flow rates were then reduced in a similar way so that the torus-shaped flame restored back to the axis. The flow rates were also recorded when the flame was restored. In select cases, axial and radial velocities were measured by means of laser Doppler velocimetry and the temperatures were measured using a coherent anti-Stokes Raman spectroscopy (CARS) system. Extensive analysis of the data obtained using different diameter tubes and nozzles over long periods of time showed remarkable consistency in the extinction strain rates. The major uncertainties arise from 1) plug flow vs parabolic flow profiles, 2) heating of the fuel and air-streams, and 3) jet separation distance. These effects have been fully accounted for in obtaining the extinction data presented here. See Refs. 4 and 15 for details.

Flame Extinction

The limitations of the present one-dimensional model deserve mention because the differences between the experiments and the analysis can be traced in part to the simplifying assumptions of the model. The one-dimensional analysis is strictly valid only when 1) the Reynolds number is large, 2) the flame zone is thin in relation to the characteristic dimension of the problem, and 3) the stagnation plane lies close to the flame zone. For ideal opposed jet configuration, the flame zone thickness must be much smaller than the diameter of the jets.[18] These criteria are not strictly adhered to in many CFDF studies. First, the flow regime of many reported experiments is in the low Reynolds number range ($\mathcal{R}_d \sim 1 \times 10^3$), which is near the lower applicable limit. Second, the flame thickness is often greater than that of the ideal thin flame. An additional, often overlooked, factor is the effect of heat release on strain rate, which appears in the axial velocity profile in Fig. 4a. The axial velocity gradient is significantly perturbed by heat release, whereas the analysis assumes a constant velocity gradient based on potential flow considerations. Obviously, this introduces some ambiguity into the appropriate value of the strain rate to be used in the analytical formulation.[6] Finally, the flame zone is not always in the proximity of the stagnation plane, especially for the hydrogen flame. Obviously, interpretation of the numerical results and comparison with experiments must take into account these limitations of the analytical formulation.

The strain rate a has been identified as the most important fluid dynamic parameter influencing the characteristics of the flame. In the present formulation, the strain rate is an input parameter determined from potential flow solution. For the axisymmetric opposed jet case, the potential flow strain rate is usually calculated using the expression

$$a = \frac{\partial u}{\partial r} = \frac{\bar{v}_{\text{jet}}}{D} \tag{19}$$

in which $\bar{v}_{\text{jet}}$ is the area-averaged jet exit velocity and D is the jet exit diameter. Similar expressions are available for other counterflow configurations such as two-dimensional jets, and cylindrical and spherical porous burners.[19] Better agreement with experiments can be achieved by applying correction factors to the potential flow strain rate defined in Eq. (20). Most of these corrections adjust the strain rate upward. Whereas, these corrections have not been widely validated, they do seem to highlight the limitations of the analytical approach and the differences among the various experimental configurations.

One parameter that controls the extinction of counterflow diffusion flame has been identified as the first Damköhler number, defined as

$$\delta = \tau_f/\tau_c \tag{20}$$

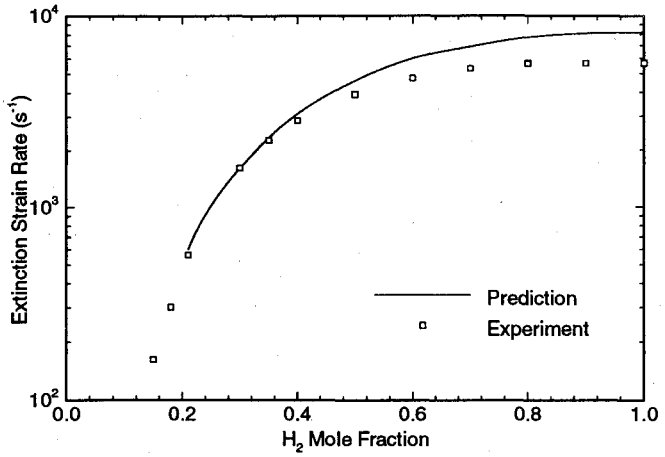

Fig. 6 Extinction curve. Experimental results from Pellett et al.[15] and computed results from the present study.

in which τ_f and τ_c represent the characteristic flow and chemical reaction times, respectively. The strain rate represents the reciprocal of τ_f. If one assumes Lewis number $Le_i = 1$, then, by measuring the extinction strain rate, one can estimate the overall reaction rate. Presently, however, the Lewis numbers are quite different from unity, and the extinction strain rate also depends on the diffusivity of the reactants. Increasing the Lewis number is equivalent to increasing diffusivity or decreasing diffusion time. Thus, the much higher extinction strain rate of the hydrogen–oxygen diffusion flame compared to the hydrocarbon–oxygen diffusion flame is because of both higher reactivity and higher diffusivity of hydrogen.

Numerical experiments were conducted to understand the influence of diffusion on extinction strain rate. For each run, the Lewis numbers Le_i for all species were assumed equal. When Le_i was parametrically varied between 1–2, the results showed that it had a dramatic effect on the extinction strain rate. For pure hydrogen, extinction occurred at $a_{ext} = 4700\ s^{-1}$, assuming $Le_i = 1$ for all species, compared to $a_{ext} = 8200\ s^{-1}$, when Le_i for each species was calculated individually using Chemkin. Therefore, for diffusion flames, the extinction strain rate can be used as a measure of overall reaction rate only when comparing reactants having the same diffusivity. In contrast, differences in the reactant diffusivities may not have such a pronounced impact on premixed flame characteristics.

Extinction is defined as the state that corresponds to a precipitous drop in temperature with a small increase in strain rate. Recently, summarized extinction results from extensive experiments are compared with the present analysis in Fig. 6. Extinction strain rates are plotted vs hydrogen mole fractions of the input fuel stream. The experimental data are from plug flow OJB (Ref. 4) instead of the parabolic flow (fully developed laminar pipe flow) OJB used in earlier experiments. The extinction results given in Fig. 6 are significant because of the close agreement between the analytical prediction and the experimental data. It should be noted that there is some uncertainty about how the potential flow strain rate is to be calculated for the different experimental configurations, and therefore, the degree of agreement between theory and experiments seen in Fig. 6 should not be expected for all experimental configurations. Extinction strain rates a_{ext}, calculated using a computer program based on a different numerical approach (Newton's method), have been reported in two recent studies[21,22] for diluted hydrogen fuel ($X_{H_2} = 0.5$). A value for $a_{ext} \sim 5000\ s^{-1}$ for axisymmetric opposed jets is reported in the former work, whereas cylindrical porous burner a_{ext} values ranging from 8600 to 11,000 s^{-1} for four different kinetic schemes are reported in the latter work.

Conclusions

A one-dimensional model has been developed independently of previous known efforts to solve the stiff equations of H_2–air counterflow diffusion flames. Development of an algorithm for the solution of the stiff equations governing hydrogen–air CFDF is an important step in understanding the associated complex phenomena. The present model uses detailed chemistry and accounts for the variation of Prandtl and Lewis numbers as well as considers the effect of thermal diffusion on the flame. The numerical procedure, based on the time-marching, finite volume approach, appears to be well suited for the present problem.

It can be inferred from the results presented that the H_2–air flame exhibits several characteristics in terms of flame location, flame structure and extinction limits, quite different from hydrocarbon flames. It is shown that, in addition to the higher reactivity of hydrogen, higher mass diffusivity also separates the H_2–air flame from hydrocarbon flames in its behavior. It is shown that the unity Lewis number assumption made in many flame studies is not realistic for the H_2–air flame; the extinction strain rate drops by a factor of 2 when the flame is simulated using this assumption. The present results show that thermal diffusion has a negligible effect on the characteristics of the flame.

The study shows that there is uncertainty regarding the chemical kinetic model most suitable for the present problem, and further work in this area would be useful. An inherent limitation of the one-dimensional model is the use of the strain rate as a known parameter of the problem, which may explain many of the disagreements between theory and experiments.

Several valuable studies may be conducted using the present analytical model. The effect of contaminants on the flame is one example. Consideration of more species, such as H_2O_2 for low temperatures, inclusion of nitrogen chemistry for high temperatures, and the use of different reaction sets can help understand the effects of chemistry on the flame. Use of the present model to investigate a recently proposed model[3] for turbulent diffusion flames, according to which turbulent diffusion flames consist of a cluster of strained, laminar diffusion flamelets, will be an interesting and challenging task for investigators interested in turbulent diffusion flames.

Acknowledgments

Financial support for this work was provided by NASA Langley Research Center under Grant NAG-1-861. We acknowledge the following contributions to the present work: Y. H. Ho wrote a large part of the original computer code used in this work as a part of his masters thesis. Lloyd Wilson, NASA Langley, did most of the extinction experiments. Robert Kee, Sandia Labs., provided the Chemkin routines. Bert Northam, NASA Langley, kept track of our progress and provided encouragement.

References

[1]Givi, P., "Model-Free Simulation of Turbulent Reacting Flows," *Progress in Energy and Combustion Science*, Vol. 15, No. 1, 1989, pp. 1–107.

[2]Givi, P., Jou, W.-H., and Metcalfe, R. W., "Flame Extinction in a Temporally Developing Mixing Layer," *Proceedings of the 21st Symposium (International) on Combustion*, The Combustion Inst., Pittsburgh, PA, 1986, pp. 1251–1261.

[3]Peters, N., and Williams, F. A., "Liftoff Characteristics of Turbulent Jet Diffusion Flames," *AIAA Journal*, Vol. 21, No. 3, 1983, pp. 423–429.

[4]Pellett, G. L., Northam, G. B., Guerra, R., Wilson, L. G., Jarrett, O., Jr., Antcliff, R. R., Dancey, C. L., and Wang, J. A., "Opposed Jet Diffusion Flames of Nitrogen-Diluted Hydrogen vs Air: Axial LDA and CARS Surveys; Fuel/Air Strain Rates at Extinction," AIAA Paper 89-2522, July 1989.

[5]Brown, T. M., Nandula, S. P., Skaggs, P. A., Pitz, R. W., Pellett, G. L., Roberts, W., Wilson, L. G., and Isaac, K. M., "Multipoint Measurement of Temperature and Species Concentrations in Opposed Jet Flames by UV Raman Scattering," AIAA Paper 94-0226, Jan. 1994.

[6]Chelliah, H. K., Law, C. K., Ueda, T., Smooke, M. D., and Williams, F., "An Experimental and Theoretical Investigation of the Di-

lution, Pressure and Flowfield Effects on the Extinction Condition of Methane-Air-Nitrogen Diffusion Flames," *Proceedings of the 23rd Symposium (International) on Combustion*, The Combustion Inst., Pittsburgh, PA, 1990, pp. 503–511.

[7]Tsuji, H., "Counterflow Diffusion Flames," *Progress in Energy and Combustion Science*, Vol. 8, No. 1, 1982, pp. 93–119.

[8]Ho, Y. H., and Isaac, K. M., "Analysis of Opposed-Jet Hydrogen-Air Counter Flow Diffusion Flame," Univ. of Missouri, MAE-TM-25, Rolla, MO, Oct. 1989.

[9]Isaac, K. M., Ho, Y. H., Zhao, J., Pellett, G. L., and Northam, G. B., "Global Characteristics and Structure of Hydrogen-Air Counter Flow Diffusion Flame: A One-Dimensional Model," AIAA Paper 94-0680, Jan. 1994.

[10]Fay, J. A., and Riddell, F. R., "Theory of Stagnation Point Heat Transfer in Dissociated Air," *Journal of the Aeronautical Sciences*, Vol. 25, No. 1, 1958, pp. 73–85.

[11]Kee, R. J., and Miller, J. A., "A Structured Approach to the Computational Modeling of Chemical Kinetics and Molecular Transport of Flowing Systems," Sandia Rept., SAND86-8841, July 1986.

[12]Patankar, S. V., *Numerical Heat Transfer and Fluid Flow*, Hemisphere, Washington, DC, 1980, Chaps. 1–6.

[13]Jachimowski, C., "An Analytical Study of the Hydrogen-Air Reaction Mechanism with Application to Scramjet Combustion," NASA TP 2791, Feb. 1988.

[14]Hahn, W. A., Wendt, J. O. L., and Tyson, T. J., "Analysis of the Flat Laminar Opposed Jet Diffusion Flame with Finite Rate Detailed Chemical Kinetics," *Combustion Science and Technology*, Vol. 27, No. 1, 1981, pp. 1–17.

[15]Pellett, G. L., Northam, G. B., and Wilson, L., "Strain-Induced Extinction of Hydrogen-Air Counterflow Diffusion Flames: Effect of CO_2, N_2, and O_2 Additives to Air," AIAA Paper 92-0877, Jan. 1992.

[16]Axelbaum, R. L., Law, C. K., and Flower, W. L., "Preferential Diffusion and Concentration Modification in Sooting Counterflow Diffusion Flames," *Proceedings of the 22nd Symposium (International) on Combustion*, The Combustion Inst., Pittsburgh, PA, 1988, pp. 379–386.

[17]Law, C. K., "Dynamics of Stretched Flames," *Proceedings of the 22nd Symposium (International) on Combustion*, The Combustion Inst., Pittsburgh, PA, 1988, pp. 1381–1402.

[18]Spalding, D. B., "Theory of Mixing and Chemical Reaction in the Opposed Jet Diffusion Flame," *ARS Journal*, Vol. 31, No. 5, 1961, pp. 763–771.

[19]Jain, V. K., and Mukunda, H. S., "The Extinction Problem in an Opposed Jet Diffusion Flame with Competitive Reactions," *Combustion Science and Technology*, Vol. 1, 1969, pp. 105–117.

[20]Katta, V. R., Goss, L. P., and Roquemore, W. M., "Effect of Nonunity Lewis Number and Finite-Rate Chemistry on the Dynamics of a Hydrogen-Air Jet Diffusion Flame," *Combustion and Flame*, Vol. 96, Nos. 1/2, 1994, pp. 60–74.

[21]Guthiel, E., and Williams, F. A., "A Numerical and Asymptotic Investigation of Structures of Hydrogen-Air Diffusion Flames at Pressures and Temperatures of High-Speed Combustion," *Proceedings of the 23rd Symposium (International) on Combustion*, The Combustion Inst., Pittsburgh, PA, 1990, pp. 513–521.

[22]Darabiha, N., and Candel, S., "The Influence of the Temperature on Extinction and Ignition Limits of Strained Hydrogen-Air Diffusion Flames," *Combustion Science and Technology*, Vol. 86, No. 1, 1992, pp. 67–85.